CHALMERS
UNIVERSITY OF TECHNOLOGY

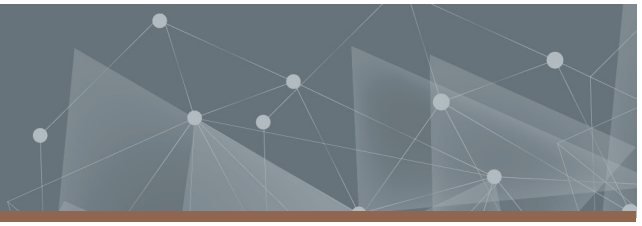

Characterization of the Forearm's Bio-acoustical Properties

A study on acoustic source localization on the human forearm as a potential human-machine interface

Master's thesis in Applied Acoustics

Niklas Brundin

DEPARTMENT OF CIVIL AND ENVIRONMENTAL ENGINEERING

Chalmers University of Technology
Gothenburg, Sweden 2021
www.chalmers.se

MASTER'S THESIS ACEX30

Characterization of the Forearm's Bio-acoustical Properties

A study on acoustic source localization on the human forearm as a potential human-machine interface

Niklas Brundin

CHALMERS

Department of Civil and Environmental Engineering
Division of Applied Acoustics
CHALMERS UNIVERSITY OF TECHNOLOGY
Gothenburg, Sweden 2021

Characterization of the Forearm's Bio-acoustical Properties
A study on acoustic source localization on the human
forearm as a potential human-machine interface
Niklas Brundin

Supervisor: Jens Ahrens, Division of Applied Acoustics
Examiner: Jens Ahrens, Division of Applied Acoustics

Master's Thesis 2021
Department of Civil and Environmental Engineering
Division of Applied Acoustics
Chalmers University of Technology
SE-412 96 Gothenburg
Telephone +46 31 772 1000

Typeset in LaTeX
Chalmers Reproservice
Gothenburg, Sweden 2021

Abstract

Bio-acoustics have started to increase in popularity outside of the medical field, where it has been used as a tool to determine bone health and provide hearing aids through bone conduction. Over the last couple of years several projects have been conducted utilizing bio-acoustical signals as an alternative to conventional human-machine interfaces such as touchscreens and voice recognition.

This thesis investigates the possibilities of utilizing the bio-acoustical characteristics of an individual's forearm as a human-machine interface through acoustic localization of self inflicted impacts. It also aims to analyze the bio-acoustical properties of the forearm, how these properties are affected by muscle tension, and to verify if these are universal properties which can be observed for multiple test subjects.

The results show that there are universal characteristics between several test subjects and that there is a frequency region between 70 Hz and 350 Hz with low attenuation, which is well suited for bio-acoustical measurements. This frequency region can be altered by having the test subjects place their wrist in extension or flexion, which causes the frequency region to shift by roughly 30%. It was also shown that the different impact positions have unique time signatures and frequency spectras compared to each other. The amplitude difference between the two sensors was also unique for the impact locations and showcased a symmetrical pattern between the medial or lateral side. The location specific amplitude differences only held true as long as impact located at the middle of the forearm were excluded. The time difference between the two sensors did not show the same symmetrical pattern as the amplitude difference, and can therefore not be used on its own to determine the direction of arrival.

Keywords: bio-acoustic, bio-vibration, bone conduction

Contents

1 Introduction

Over the past decades there have been tremendous achievements accomplished in developing human-machine interfaces as a response to the advancements in technology. Some of the recent breakthroughs have been touchscreens and voice recognition which, although successfully helped expand the human-machine interface, still suffer limitations. Voice recognition has trouble functioning in environments with loud background noise as well as causing privacy concern when interacted with in public. Touchscreens are limited in size of the screen, which has caused limited usability for accessories such as smart watches. A way to expand or even replace these human-machine interfaces would be to incorporate the user's own body through bio-acoustical signals. This thesis will investigate the possibility of having the forearm of a person function as an input device through acoustical localisation of self inflicted impacts of the forearm.

1.1 Background and previous work

Bio-acoustics will, within this report, be referring to acoustical signals traveling through the human body in the form of vibrations. Bio-acoustics have previously been utilized in several fields within medicine, including hearing aids based on bone conduction as well as being utilized as a useful tool to determine bone health of patients with Osteoporosis. Besides the medical applications there has also been some projects using bio-acoustics as an alternative way of transmitting data.

One of the projects regarding data transmission is *Hambone*, which is a bio-acoustic gesture interface that utilizes vibrations caused by body movements, as a human-machine interface. *Hambone's* setup consists of piezoelectric sensors located at the wrist which picks up the sound caused by hand movements traveling through bone. If the energy of the vibrations exceeds a threshold, the system will start recording vibrations and map the measured data with a library of pre-recorded hand movements. Although this project is very impressive, design flaws led to a delay of several seconds, which leaves room for improvement [1].

Another project regarding data transmission is *OsteoConduct*, which is designed to be an alternative to other wireless technologies such as Bluetooth. As Bluetooth has a high power consumption, *OsteoConduct* presents bio-acoustical signals as a viable alternative. The technology utilizes the human musculoskeletal system to transfer data by mechanically exciting bone conduction, which causes vibrations to travel through the body. The project looked into using different body parts such as the forearm with promising results, where a system built into a wrist watch could be used to detect the vibrations. The concept was then used to construct a user interface where the user excited vibrations through teeth clacks which traveled through the body before being picked up by a body worn device [2].

The project *Skinput* utilizes the vibrations transferred through the skin and bones of an individual's forearm as an input device. By having sensors mounted to the individual's arm with an armband, taps on the skin can be tracked to localize the impact location. This is done by pre-record vibrational patterns of the forearm, which is then linked to certain segments of the skin. This system is then combined with a pico-projector in order to create an interactive graphical interface located on the forearm. This project is fairly similar to the study conducted in this thesis, with the exception of the usage of pre-recorded vibrational patterns to train a machine-learning algorithm [3].

1.2 Aims

The aim of this project is to look into the possibility of constructing a system which can localize the impact location of an individual's forearm using bio-acoustical signals. This is broken down into five goals:

- Look into previous studies and projects related to this field. The findings from these will then be used for both constructing the test cases of this project, as well as providing measurement results which can be compared to the ones obtained in this project.

- Construct a test environment which can both excite and measure the frequency characteristics of a forearm.

- Conduct measurements on the forearm with different wrist positions. This will showcase how much muscle tension affects the frequency characteristics of the forearm.

- Perform measurements on several test subjects. This will help determine if the frequency characteristics of the forearm is universal or unique for every individual.

- Investigate if there are location specific time and frequency characteristics on the forearm that can be used to obtain the impact location without the need of advanced algorithms. This will be done by self inflicted impacts on the forearm which will be analysed by looking at the amplitude differences, time delay variations as well as frequency characteristics between the different impact locations.

2 Theory

Through body movements and impacts inflicted on the body, bio-acoustical signals can be created and transmitted through the bones, skin and joints of a person. These signals can travel with enough strength to be readable by sensors located on other body parts than the one they originate from [2]. These bio-acoustical signals have been analyzed and utilized in several studies and projects over the last decades, although further research in this field is clearly wanted.

This chapter aims to present the reader with the basics of bio-acoustics, how it has been used in previous reports and studies as well as how they operate within the forearm.

2.1 Bio-acoustics of the forearm

2.1.1 Anatomy of the forearm and its bio-acoustic properties

The forearm consists of two long bones stretching from the elbow, where they join with the humerus, to the wrist where they join with the carpal bones. These two long bones are called the radius and the ulna, where the radius is the thicker of the two, located on the lateral side of the forearm, and the ulna is located on the medial side of the forearm. The bones consists of three main types of tissue; the compact bone tissue located at the outside of the bones (a very stiff and rigid tissue with small tunnels leading blood vessels and nerves), the softer, more light and porous bone tissue, and the semi-solid bone marrow. The wrist joint is of the type condyloid, which means that it allows circular motion as well as flexion and extension, and is held in place by numerous ligaments. The joint also contains cavities with the lubricating non-Newtonian synovial fluid [4] [5].

The soft tissue surrounding the long bones of the forearm all have a relatively high dampening factor compared to the stiffer and more compact bone. This leads to a large

attenuation and thus a poor transmission of vibrational energy, especially in higher frequencies. Muscles, compared to the other soft tissues, possess the ability to create tension by shortening its fibers, leading to a contraction. Several studies has shown that the increased muscle tension of the forearm will affect the frequency characteristics of the forearm. *Jurist* conducted measurements on the Ulna with the forearm in neutral position, at maximal forearm supination as well as with maximum gripping effort. The findings showed that the resonance frequency increased with roughly 20% for the supinated position, while the gripping effort increased the resonance frequency with roughly 5% [6]. *OsteConduct* also showcased that muscle contractions pushed the frequency ranges with lowest attenuation towards slightly higher frequencies [2].

As sound velocity is dependent on both density and elastic properties of solid mediums in which it travels through, there will be large differences between the speed of sound in the bones of the forearm and the soft tissues surrounding them. This means that the acoustical distance in which the bio-acoustical signals travels through for each tissue type will affect the time it takes for the signals to traverse through the forearm [7]. It is also possible for the density of the bone tissue to vary between different segments, leading to a variation in the speed of sound between the segments. This causes the time it takes for a bio-acoustical signal to travel a fixed distance to be dependent on its path, even though it is the same type of tissue it moves through. *Clayton Rich et. al* found in their study *"Sonic Measurement of Bone Mass"*, where measurements were conducted on beef bone, muscle and fat, that there is a large difference between the speed of sound in these tissues. The results showcased that the speed of sound in bone to be 2880 m/s, 1630 m/s for muscle and 1540 m/s for fat [7]. The speed of sound in homogeneous tissue will vary from non-homogeneous tissue. This means that fatty tissue will have a lower speed of sound compared to muscle, but still have a greater speed of sound compared to pure fat.

2.1.2 Bio-acoustical propagation of the forearm

By externally exciting the forearm through physical impact on its skin, the energy from the impact will create vibrations which will be dispersed. Some of the energy will be lost as radiating acoustical sound waves propagating to the surrounding air, while most of the energy will be transmitted through the forearm. The transmitted energy will mainly consist of two types of vibrations, transverse waves and longitudinal waves [3]. The transversal waves will follow the surface of the skin, propagating outwards from

the impact location. As these are created by the displacement of soft tissue, their amplitude is directly correlated to the amount of soft tissue located at, and close to, the impact location as well as the force of the impact. These are illustrated in Figure 2.1.

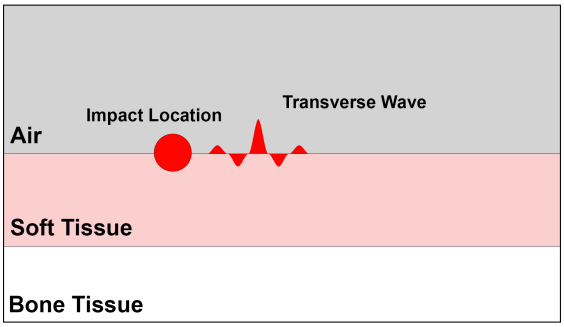

(a) Transverse wave propagation at time t=1

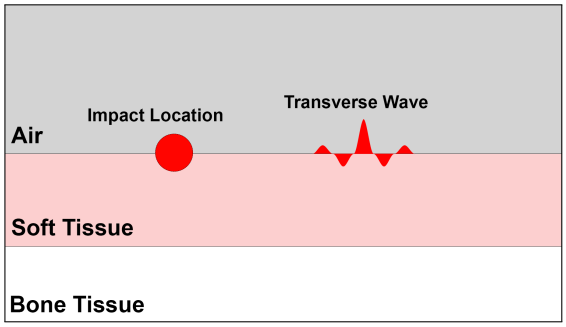

(b) Transverse wave propagation at time t=2

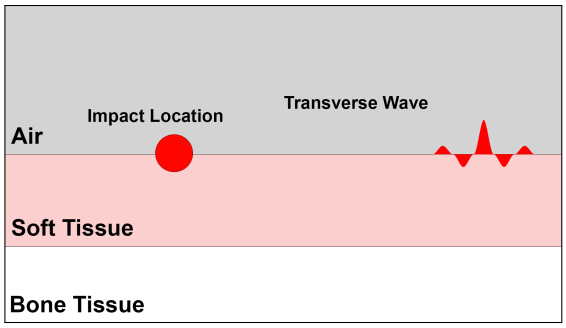

(c) Transverse wave propagation at time t=3

Figure 2.1: Transverse wave propagation caused by skin displacement

The longitudinal waves created by the impacts on the forearm will travel downwards until they reach and excite the bones. As bones are stiff and less deformable

compared to the surrounding soft tissue, the dampening factor will be much lower, allowing the vibrational energy to be transmitted over longer distances and eventually spread through the whole bone. Just as the vibrational energy went from the soft tissue to the bone, the opposite where the vibrations from the bone excites the soft tissue will occur. This will create a complex interchange of vibrations between the bone and the soft tissue [3]. This is visualized in Figure 2.2.

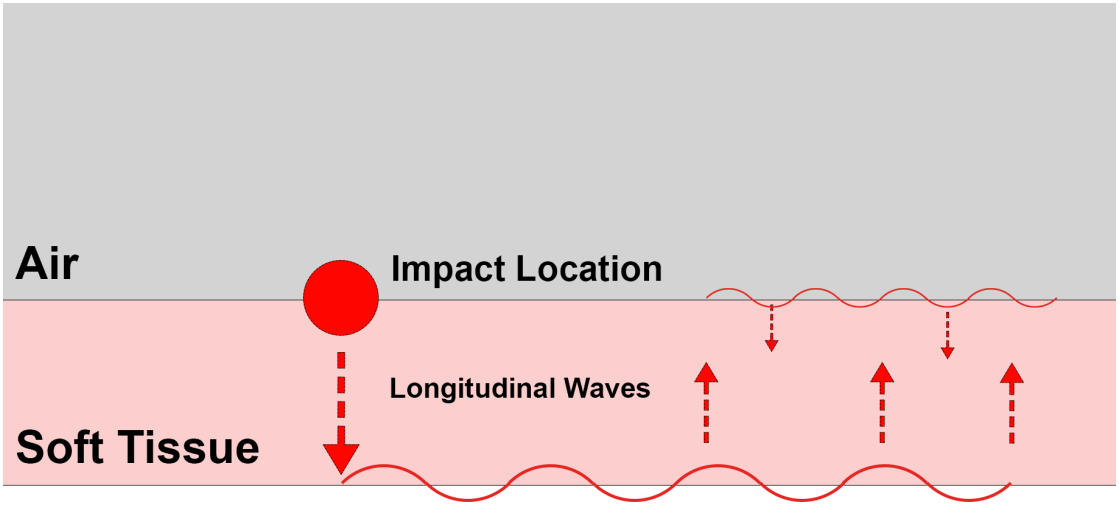

Figure 2.2: Longitudinal wave propagation and exchange of vibrational energy between bone and soft tissue

As mentioned in Section 2.1.1, the coupling between the bones consists of ligaments and joints filled by synovial fluid. The authors of *Skinput* hypothesized that these will dampen specific frequencies and thus act as acoustical filters between the bones [3]. They believe that this is what makes it possible to track, from which finger vibrations on the wrist originates from, as this will create location-specific acoustic signatures depending on the vibrational path. This is probably what allows other successful projects, such as *Hambone* which tracks the bio-acoustical signals created by hand gestures and compares these with a library of pre recorded gestures, to function so well [3] [1].

2.2 Bio-acoustical measurements and bone-conducted vibrations

2.2.1 Sensor mounting

The stiffer an accelerometer is mounted to a structure, the larger the readings of the sensor will be. This is why stud-mountings or beeswax if often used to couple the accelerometer with the structure. For bio-acoustical measurements conducted on living participants, studs are not feasible and beeswax is unpractical. This means that the sensors needs to be held down by a structure or to be held in place using double adhesive tape, which will by nature limit the readings of the sensors [8].

For projects such as *Hambone*, which has utilized skin mounted sensors to measure bone vibrations, it has been stated that the sensors need to be mounted as rigid as possible to the bone of interest. Since the bone will always be covered by soft tissue, it can become problematic as large volumes of soft tissue is pushed aside, creating a crater of soft tissue surrounding the sensor and thus alter the acoustical behavior of the arm. It is also a risk that the sensor moves while conducting the measurements if the skin at the measurement location is too loose. Therefore the best locations to conduct bio-acoustic measurements on bone conductivity are places with very little soft tissue, while at the same time having minimal amount of loose skin. These criteria are met on both the elbow as well as the ulnar and radial styloids (the bumps of the wrist) [1]. This, in combination with how easily accessible the forearm is, has made it the focus of several studies within bio-acoustics.

2.2.2 Bio-acoustics as bone-conducted vibrations

Sound wave propagation has been used in several different medical fields and has especially been helpful in aiding patients with hearing loss. As the usage of bone-conducted hearing aids has grown in popularity, it has been proven that bone is capable of transmitting vibrations throughout the frequency range of human speech [3]. This has lead to bone-conducted hearing aid designs transmitting vibrations from the outer ear to the inner ear without the need of signal modifications [2]. Besides using bio-acoustics to treat hearing loss, it has also been used for diagnosing the bone health of patients with Osteoporosis. As the bone loses density its acoustical properties changes, which can

be detected through bio-acoustical measurements. This is done by exciting and measuring the bone which then provides structural data, such as the speed of sound and Young's modulus [9] [10] [6]. The operational frequencies of the systems conducting these measurements are located within the ultra sound range, which comes with an inherent shallow penetration depth and causing sound wave propagation to only lie within a few millimeters from the excitation point. In order to transfer bio-acoustical signals over longer distances, the operational frequency needs to be lower. This will also bring the frequencies closer to the resonance frequency of the long bones, which will excite the whole arm and thus transmitting a stronger signal [2].

2.3 Modeling the vibrational characteristics of a long bone and in vivo Measurement Results

The vibrational characteristics of a long bone can be described in the same way as a vibrating bar [6]. For longitudinal waves this is usually done with the following equation

$$C = \sqrt{\frac{B + \frac{4}{3}G}{\rho}} \tag{2.1}$$

where C is the speed of which longitudinal waves propagate through the bar, B and G are the bulk modulus and shear modulus of the bar, and ρ is the average density of the bar [11]. This equation works well for high frequencies where the wavelengths are shorter than the diameter of the bar. Due to the size of human long bones, this will cause a problem when analyzing lower frequencies, which is why the fundamental equation for vibrational properties seen in Equation 2.2 can be used instead.

$$F_0 L = KC \tag{2.2}$$

In Equation 2.2, F_0 is the resonance frequency of the bar, L is the length of the bar, K is a constant of proportionality dependent on the mode of vibration and boundary conditions [12]. Similar to the longitudinal waves, the formula seen in Equation 2.3 can be used to describe transverse waves of a bar

$$F_0 L = kv \tag{2.3}$$

where F_0 is the transversal resonance frequency, L is the length of the bar, k is a proportionality constant and v is the transversal waves phase velocity. The transverse phase velocity of a bar can itself be described through Equation 2.4

$$v = \sqrt{2\pi FCR} \tag{2.4}$$

where F is a frequency, C is the speed of sound inside the bar and R is the radius of the cross section about the neutral axis of the bar [6]. By combining Equation 2.4 and Equation 2.3, the expression seen in Equation 2.5 can be derived.

$$F_0 L = \frac{2\pi k^2 R}{L} C \tag{2.5}$$

With the assumption that all people have the same ratio for their long bones, $\frac{R}{L}$, Equation 2.5 can be rewritten as seen in Equation 2.6.

$$F_0 L = k^* C \tag{2.6}$$

For Equation 2.6, k^* is a new constant of proportionality defined in Equation 2.7.

$$k^* = 2\pi k^2 \frac{R}{L} \tag{2.7}$$

The clear resemblance between Equation 2.6 and Equation 2.2, as well as the fact that both k^* and K are arbitrary proportionality constants, a general equation can be created as seen in Equation 2.8.

$$F_0 L = KC \tag{2.8}$$

This general equation can be used to describe the vibrational properties of a resonating long bone as long as K is treated as a function of boundary conditions of the bone, geometry of the bone as well as the mode of vibration [6].

Equation 2.8 is based on several assumptions which may cause it to deviate from physical measurements. For instance, as the bone impedance is much larger than that of soft tissue in lower frequencies, any coupling effect has been neglected. It is also assumed that the long bone is a uniform cylinder with the same thickness and density throughout the whole length of the bone. The joints are also treated as true hinges, which is not the case [6]. With all of the above in mind, any calculated resonance frequency should be treated as a rough estimate and not a precise prediction. For these calculations, the speed of sound, C, can be estimated to be close to 2900 m/s, as discussed in Section 2.1.1.

Jurist used Equation 2.8 to calculate the transversal resonance frequency to be 230 Hz by modeling the ulna as a cylinder with a length L of 0,3 m, and an inner and outer radius of 0,033 L and 0,05 L. This was shown to correspond well with the results from *Jurist's* in vivo measurements of the Ulna, which occurred around 250 Hz [6]. *OsteConduct* also conducted in vivo measurements, and found that the differences between test subjects lead to variations in where the resonance occurs, which took place between 150 Hz and 300 Hz [2]. In vivo studies have also shown that there are more than one resonance taking place within a long bone, which can be explained through several vi-

brational modes in the bone. The extra resonance is typically located around 450 Hz for the ulna, and for other long bones such as the tibia, the modes have been shown to occur around 130 Hz, 290 Hz and 560 Hz [13] [6]. The region with the least attenuation for the ulna is located between 150 Hz and 350 Hz, which has been seen to work well for other bones in the body as well [2].

2.3.1 Signal analyses

The following section presents some of the signal processing and analyzing tools used to obtain the results throughout this report.

Single-sided auto and cross-spectrum

The auto and cross-spectrum, also known as the auto and cross-spectral density, are measurements of the power distribution over frequencies. The squared amplitude of each frequency component contained in a time signal corresponds to the power spectrum's values. The autospectrum is generally used when analyzing signals since it is showcasing the power of the signal while the cross-correlation is often used to reduce uncorrelated noise between two signals [14].

The autospectrum of a signal is calculated through

$$S_{xx} = X(\omega)\overline{X}(\omega) \tag{2.9}$$

where S_{xx} is the autospectrum of the Fourier transformed signal $X(\omega)$, $\overline{X}(\omega)$ is its conjugate and ω is the angular frequency. Similarly, the cross-spectrum can be calculated through

$$S_{yx} = Y(\omega)\overline{X}(\omega) \tag{2.10}$$

where S_{yx} is the cross-spectrum between the two Fourier transformed signals $Y(\omega)$ and $X(\omega)$. As the Fourier transformed signals will include both the positive and negative frequency information, it is common to convert the results into single-sided spec-

trum which only contains the positive frequency information. This can be done by simply discarding the negative frequencies and correcting the positive frequency components amplitudes, except for the frequency components at 0 Hz and at the Nyquist frequency, to still represent the correct signal energy. As the negative frequency components will have an amplitude equivalent to the conjugate of the mirrored positive frequency components, the positive frequencies can be corrected by multiplying with a factor of two [14] [15].

Signal to noise ratio

The ratio between the average power of the signal and the noise floor is referred to as the signal to noise ratio, SNR. This ratio can be useful when analyzing the quality of a measurement, as a low SNR will indicate undesired noise in measurement data.

Due to the dynamic range of signals, the signal to noise ratio is often presented in logarithmic scale according to

$$SNR_{dB} = 10log_{10}\left(\frac{P_{Signal}}{P_{Noise}}\right) \tag{2.11}$$

where SNR_{dB} is the SNR presented in logarithmic scale, P_{Signal} is the power of the signal and P_{Noise} is the power of the noise. By using the quotient rule for logarithms the formula can be rewritten as

$$SNR_{dB} = 10log_{10}\left(P_{Signal}\right) - 10log_{10}\left(P_{Noise}\right) \tag{2.12}$$

By conducting measurements both with and without an active signal and plotting these over the same frequency axis, it is possible to obtain a SNR based on the level difference between these for each frequency, if the assumption is made that the background noise is static.

Transfer function and coherence

The relation between the input and output signal can be described through

$$Y(\omega) = H(\omega)X(\omega) \tag{2.13}$$

where $Y(\omega)$ is the output signal, $H(\omega)$ is the transfer function (sometimes refferred to as the frequency response function) and $X(\omega)$ is the input signal of a system. The transfer function describes the characteristics of a system independent of stimulating energy, and can from Equation 2.13 be calculated through Equation 2.14 [14] [15].

$$H(\omega) = \frac{Y(\omega)}{X(\omega)} \tag{2.14}$$

As measurements of systems often include noise, especially at the output, it follows that the transfer function calculated through Equation 2.14 may deviate from the physical systems transfer function. To counter this it is possible to calculate an estimated transfer function based on the signals cross-spectrum which will reduce uncorrelated noise. The underestimated transfer function can be calculated through

$$H_{yx,1}(\omega) = \frac{G_{yx}(\omega)}{G_{xx}(\omega)} \tag{2.15}$$

where $H_{yx,1}(\omega)$ is the underestimated transfer function, $G_{yx}(\omega)$ is the single-sided cross-spectrum between the output signal $Y(\omega)$ and the input signal $X(\omega)$, and $G_{xx}(\omega)$ is the single-sided autospectrum of the input signal $X(\omega)$. Similarly, the overestimate transfer function can be calculated through

$$H_{xy,2}(\omega) = \frac{G_{yy}(\omega)}{G_{xy}(\omega)} \tag{2.16}$$

where $H_{xy,2}(\omega)$ is the overestimated transfer function, $G_{yy}(\omega)$ is the auto correlation of the output signal $Y(\omega)$ and $G_{xy}(\omega)$ is the single-sided cross-spectrum between the input signal $X(\omega)$ and the output signal $Y(\omega)$. The underestimated transfer function will counteract uncorrelated noise at the output of the system, while the overestimated transfer function will reduce the uncorrelated noise at the input of the system [15].

The coherence function showcases how well the stimulus energy and the response energy correlates, and is therefore a useful tool to indicate the transfer functions' quality. The coherence function is calculated through

$$\gamma_{xy}^2(\omega) = \frac{|G_{xy}(\omega)|^2}{G_{xx}(\omega)G_{yy}(\omega)} \tag{2.17}$$

where $\gamma_{xy}(\omega)$ is coherence function, and $G_{xy}(\omega)$, $G_{xx}(\omega)$ and $G_{yy}(\omega)$ are the single-sided cross-spectrum and autospectrums of the Fourier transformed signals $X(\omega)$ and $Y(\omega)$ [14].

Frequency responses and conversion to mobility

When conducting vibrational measurements, three common functions used to analyze the frequency response are Compliance, Accelerance and Mobility. These functions all contain the same information of the vibrational response from a dynamic excitation force, but are based on different units of motion [16]. Compliance is based on displacement according to

$$H(\omega) = \frac{X(\omega)}{F(\omega)} \tag{2.18}$$

where $H(\omega)$ is the compliance in $\frac{m}{N}$, $X(\omega)$ is the displacement in m and $F(\omega)$ is the dynamic input force in N [16]. Mobility is based on velocity according to

$$M(\omega) = \frac{v(\omega)}{F(\omega)} \tag{2.19}$$

where $M(\omega)$ is the mobility in $\frac{m}{Ns}$ and $v(\omega)$ is the velocity in $\frac{m}{s}$ [16]. Accelerance is based on acceleration according to

$$A(\omega) = \frac{a(\omega)}{F(\omega)} \tag{2.20}$$

where $A(\omega)$ is the accelerance in $\frac{m}{Ns^2}$ and $a(\omega)$ is the acceleration in $\frac{m}{s^2}$ [16].

As all of the motion units are related through algebra, it is easy to convert between the different frequency response functions while still keeping the magnitude and phase data. This means that for any measurements conducted with accelerometers, which is

the case for this project, the measured acceleration can be used to calculate the acceleerance which in turn can be integrated in order to obtain the mobility [17] [16].

3 Lab setup and test implementation

In order to perform the necessary measurements for this project, a lab setup was constructed at Chalmers department of Sound and Vibrations. This setup was then used for all measurements leading to the results of this report. The following chapter describes this lab setup as well as all the measurements conducted with it.

3.1 Lab setup and used equipment

The lab setup which was used to conduct the measurements for this project consisted of several pieces of lab equipment which are listed in Table 3.1. Figure 3.1 showcases how the different pieces of equipment are connected to each other.

List of equipment	
Type	**Model**
2x Accelerometers	B&K type 4517
Amplifier	Yamaha M-35
Calibrator	B&K type 4294
Conditioning amplifier	B&K type 2635
Data acquisition unit	National Instruments type 9234
Force transducer	B&K type 8203
Shaker	B&K LDS V101
Stinger (40 mm)	-
MathWorks software	Matlab

Table 3.1: List of used equipment

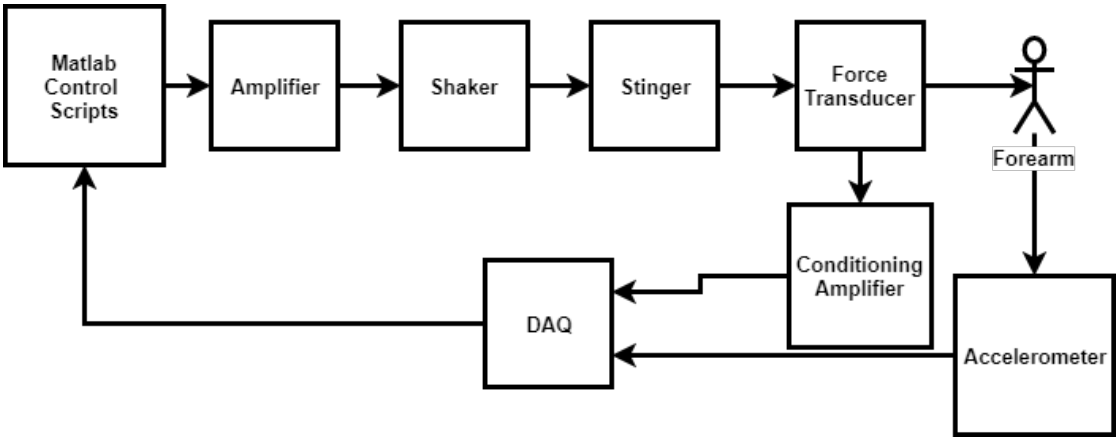

Figure 3.1: Block diagram of the lab setup

The input signal of the system was generated through *MathWorks'* software *Matlab*. The signal was then treated by an amplifier before reaching the shaker, which converted the electrical signal into mechanical vibrations. The vibrational output of the shaker was then fed through a stinger before reaching a force transducer which was mounted on top of the forearm.

As the vibrations from the shaker were lead through the stinger and force transducer onto the surface of the forearm, the vibrations excited the skin and bones of the forearm and created bio-acoustical signals as described in Section 2.1.2. These signals were then carried through the forearm until they reached the accelerometers, mounted on top of the forearm. The output of the force transducer and the accelerometers were then fed to the data acquisition unit, DAQ, where they were synchronized. Before reaching the DAQ, the output of the force transducer was amplified through an analog conditioning amplifier. The delay from this path was assumed to be minuscule and therefore neglected. The output of the DAQ was then fed into the computer running the *Matlab* measurement scripts, where they were stored for future processing and analyze. During each measurements the forearm of the test subject was placed on top of two armrests, supporting the forearm at both the elbow and wrist. Figure 3.6 displays some photos of the measurement setup.

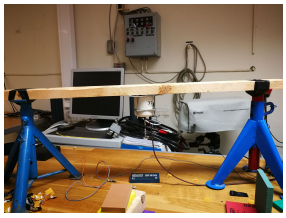

Figure 3.2: Shaker mounting structure

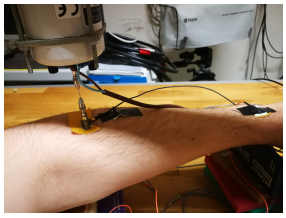

Figure 3.3: Shaker and sensor mounting

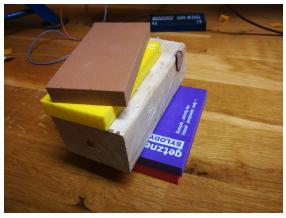

Figure 3.4: Armrest used for elbow placement

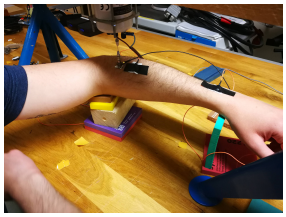

Figure 3.5: Full measurement setup

Figure 3.6: Visual presentation of the measurement setup

As discussed in Section 2.2.1, it is important for the sensors to have rigid mounting with the forearm during the measurements in order to obtain good measurement results. This is also true for the stinger and force transducer in order to excite the bone properly, as these pass the energy from the shaker to the forearm. At the same time, Section 2.2.1 brings up how the pre-stress on the forearm can alter the frequency characteristics of the forearm. Because of this, the shaker was mounted with different pre-stresses to find the best setup. Having a loose mounting provided a very weak signal at the accelerometers. This is probably due to the bone not being properly excited combined with the larger dampening factor of the skin, as mentioned in Section 2.1.1. A more rigid mounting of the force transducer against the bone provided much better results, but there is a clear crater of soft tissue created by the pre-stress. This probably affected the skin conduction as the soft tissue surrounding the force transducer created a crater. Since this provided the best signal strength for the accelerometers, it became the standard mounting for the measurements utilizing the shaker.

3.2 Uncertainties of the measurement setup

As the bio-acoustical measurements were conducted on the forearm using accelerometers and force transducers, any airborne acoustical interference was neglected. Structure born vibrations were still seen as a potential risk which could interfere with the results. Bio-acoustical vibrations have a tendency to travel throughout the whole body once they have been created, as mentioned in Section 2. This implies that any body movement caused by the test subject, even from body parts that are not directly linked to the forearm, could interfere with the measurements being conducted on the forearm. Due to this, all test subjects were told to be as still as possible during any measurements and not to talk.

Besides bio-acoustical vibrations originating from other body parts obstructing the measurements, it became clear that the test setup itself could interfere with the measurements as the whole structure seems to have had a resonance frequency around 270 Hz, the same region which the forearms resonance was expected to occur according to Section 2.3. For the vibrational energy of the structure to reach the sensors on the forearm, it would have to travel a long path with several material changes compared to the primary path, where the vibrational energy from the shaker would be directly fed to the forearm through a stinger. Therefore it was assumed that even if any vibrations from the structure would have reached the sensors, they would have been much lower in magnitude compared to the primary path and thus neglectable.

Due to the design of the test setup and with the varying amount of soft tissue on the test subjects forearms, the pre-stress of the force transducer and shaker was not constant between measurements. This probably affected the bio-acoustics of the forearm since the soft tissue surrounding the mounting position of the force transducer formed a small crater as it was pushed into the skin by the stinger. It is unclear how much of an impact this actually had on the test results.

3.3 Test procedure

The measurements of this project were conducted using the lab setup described in Section 3.1. The generated signals that was passed through the forearm consisted of two different signals. The first was a sweep signal ranging between 10 Hz and 1500 Hz for a time duration of 300 seconds, and the second consisted of white noise for a dura-

tion of 300 seconds. The results of these measurements were later processed to obtain the various parameters used to analyze the vibrational properties of the forearm. The following subsections will describe how each measurement was conducted.

3.3.1 Sensor verification and bio-acoustical properties of the forearm

For these tests the measurement setup consisted of placing one accelerometer at the radial styloids, the force transducer at the top of the forearm close to the elbow joint, as well as a second accelerometer five centimeters from the force transducer between the first accelerometer and the force transducer as seen in Figure 3.5.

The measurements were then conducted without any input signal as well as with the generated signals mentioned in Section 3.3. The measurement without any signal was conducted in order to obtain the noise floor of the whole system, including electrical interference from the measurement equipment as well as bio-acoustical noise in the forearm. This could then be compared to the measurements conducted with input signals to determine the level difference between the noise floor and the active signal. The measurement data obtained through the generated signals was also used to obtain results such as auto spectrum, coherence and transfer function.

3.3.2 Wrist position and bio-acoustics

As mentioned in Section 2.1.1, a large portion of the soft tissue of the forearm consists of muscles which has the inherent ability to create tension, and thus alter its acoustical properties. This comes natural as a point of interest for this project, which is why the forearm was measured with the forearm in flexion, extension and neutral position, visualized in Figure 3.7.

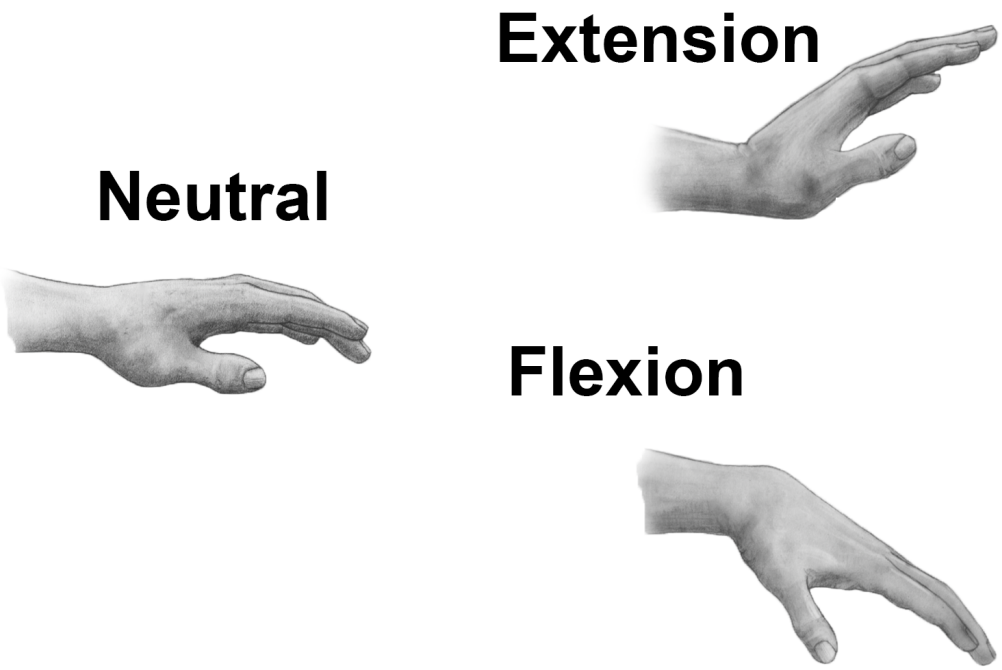

Figure 3.7: Different wrist positions

For this measurement the force transducer was placed on the middle of the forearm close to the elbow. One of the accelerometers was placed on top of the radial styloids, while the second accelerometer was placed on the skin between the first accelerometer and the force transducer, five centimeters from the force transducer, creating a straight line of sensors following the bones of the forearm.

The goal of these measurements were to see how much the difference in muscle tension caused by the extreme wrist positions would have on the bio-acoustical properties of the forearm compared to the neutral position.

3.3.3 Measurements on multiple test subjects

As the resonance frequencies of long bones are dependent on the geometry of the bone, as discussed in Section 2.3, combined with the inherent variation in bone density and soft tissue between individuals, it is of interest to measure the bio-acoustical properties

of the forearm on several test subjects. This will help determining how much the bio-acoustical characteristics vary between test subjects.

The measurements were conducted on a unfortunately rather homogeneous test pool of four test subjects. All of the participants were males in their mid twenties and with similar lengths of their forearms. Table 3.2 presents the test subjects with their gender, age, forearm length and calculated resonance, based on Equation 2.8 with the assumption that all participants have similar radius of their ulna. Even though these measurements will not showcase how much the characteristics can vary between extreme cases, it is a good comparison to see how much variation will take place for similar test subjects.

Test Subject	Gender	Age	Length of Forearm	Calculated Ulna Resonance
Subject #1	Male	24	0,28 m	243 Hz
Subject #2	Male	29	0,24 m	283 Hz
Subject #3	Male	27	0,29 m	235 Hz
Subject #4	Male	25	0,28 m	243 Hz

Table 3.2: Test pool participants

For this measurement the force transducer was placed on the middle of the forearm close to the elbow. One of the accelerometers was placed on top of the radial styloids, while the second accelerometer was placed on the skin between the first accelerometer and the force transducer, five centimeters from the force transducer, creating a straight line of sensors following the bones of the forearm.

3.3.4 Multiple impact locations and location-specific acoustic signatures

By having an accelerometer located at each of the radial styloids, the test subject used their other hand to firmly tap on fifteen different locations of the forearm. Each location was repeatedly tapped with a few seconds between each impact to have the vibrations settle. This was then repeated for all fifteen positions showcased in Figure 3.8.

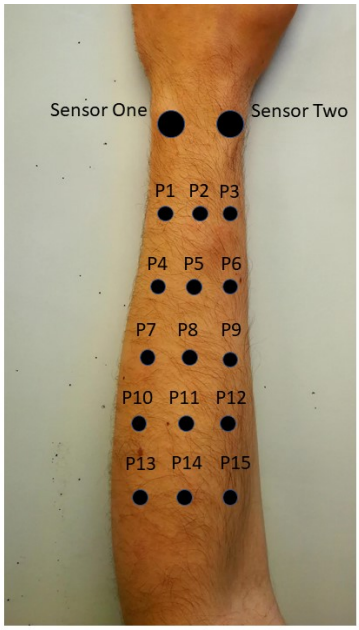

Figure 3.8: Impact locations

These measurements were conducted in order to analyze the location-specific acoustic signatures from each impact location. This was done to showcase differences both in time and frequency spectra between the impact locations and sensors, as discussed in Section 2.1. As the exciting impacts are self inflicted, there will be a variation in input force between each impact.

4 Results

4.1 Sensor verification and bio-acoustical properties of the forearm

The results presented in this section was obtain through the measurements described in Section 3.3.1, and were conducted in order to both compare the signal strength to the noise floor, as well as obtaining some bio-acoustical parameters of the forearm.

The sensors were placed according to what is described in Section 3.3.1. Through out this section the accelerometer located at the radial styloids will be referred to as Sensor two, while the accelerometer placed between the force transducer and Sensor two will be referred to as Sensor one.

The results presented were calculated according to the what is described in Section 2.3.1.

4.1.1 Noise floor and auto spectra

Figure 4.1 compares the single-sided auto spectrum for Sensor one, with both the idle signal and active white noise signal. The level difference lies between 16 dB to 40 dB over the frequency region analyzed. It also appears as the frequency region between 100 Hz and 400 Hz contains the most energy for the active signal.

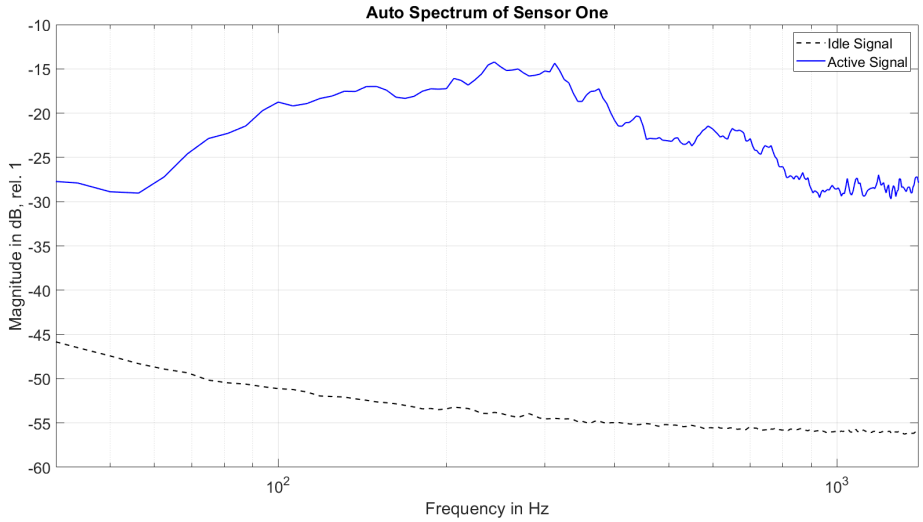

Figure 4.1: Signal strength comparison between idle and active signal of Sensor one

Figure 4.2 showcases the auto spectrum of the idle and active white noise signal at Sensor Two. The signal strength falls very low at higher frequencies where it differs by less than 5 dB from the idle measurement. There seems to be two resonances around 160 Hz and 400 Hz.

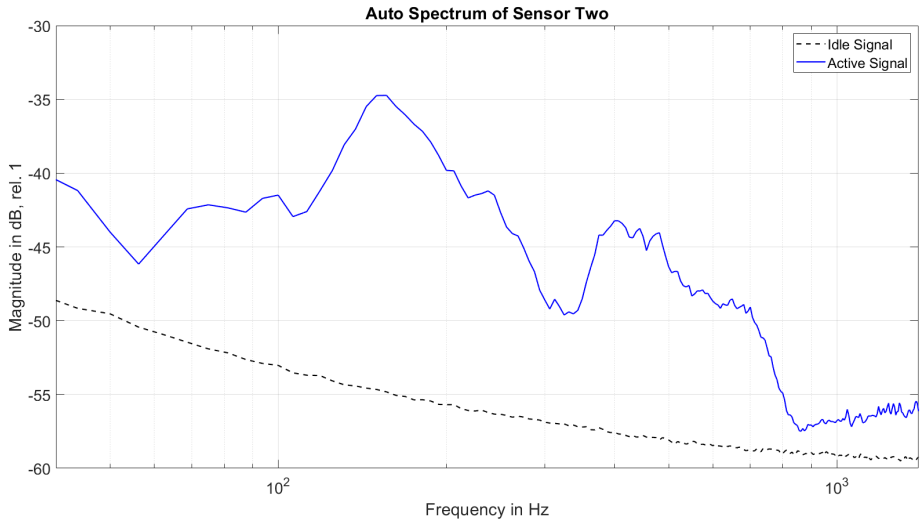

Figure 4.2: Signal strength comparison between idle and active signal of Sensor Two

The single-sided auto spectrum for the force transducer can be seen in Figure 4.3 for both the idle signal and the signal with white noise. The level of the active signal is much stronger compared to the noise floor for all frequencies and the input energy seems to stay relatively flat between 80 Hz and 200 Hz. There is a resonance in the idle signal at 50 Hz, which is probably due to electrical interference. Even at this resonance the active signal is still close to 10 dB stronger.

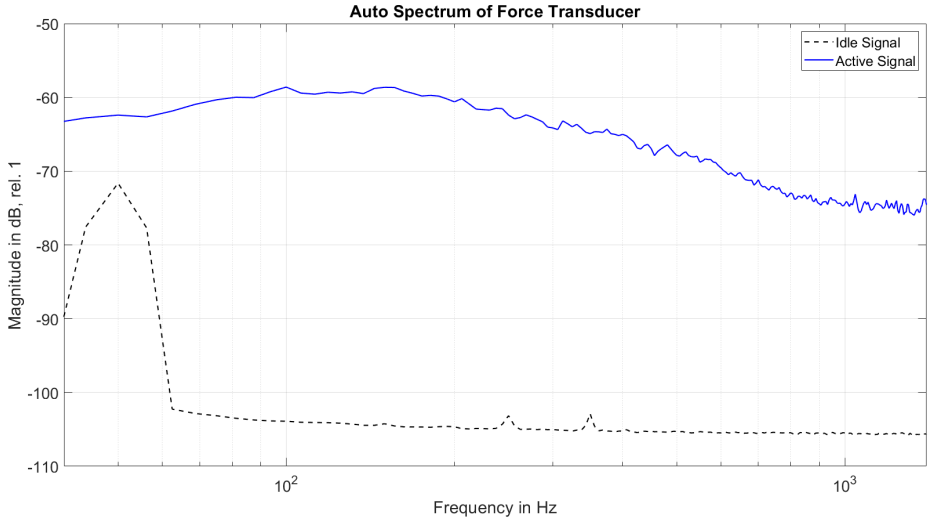

Figure 4.3: Signal strength comparison between idle and active signal of Force transducer

4.1.2 Coherence

Figure 4.4 showcases the coherence between the different sensors, obtained through the white noise measurement. Both of the sensors have a good coherence between 70 Hz and 700 Hz with the exception of a dip around 300 Hz which is present for both coherence plots containing Sensor one.

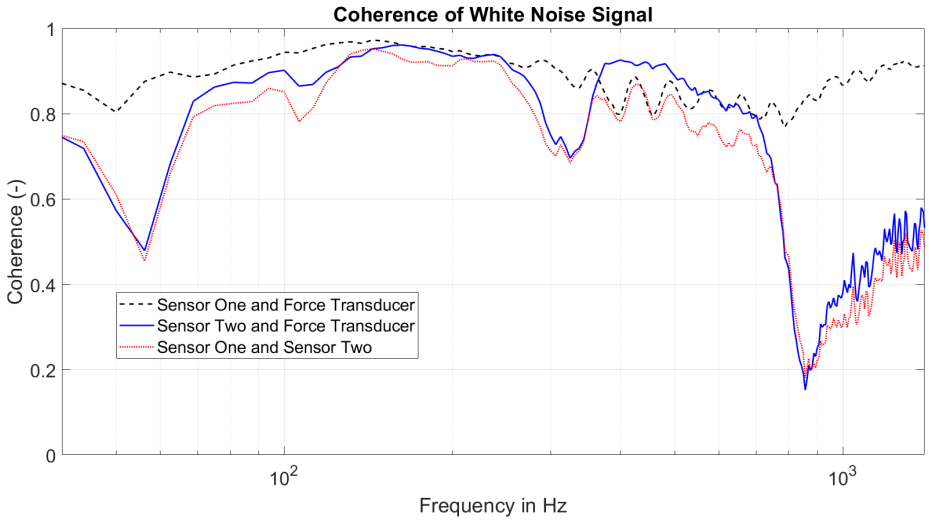

Figure 4.4: Coherence from the active white noise signal between the different sensors

4.1.3 Transfer function

The transfer functions based on the sweep signal can be seen in Figure 4.5. They seem to have several peaks and dips throughout the whole frequency region, but none is as prominent as the dip occurring around 280 Hz. This dip corresponds well with the coherence dip at the same frequency in Figure 4.4 as well as the dip between the two peaks seen in the auto spectrum plot for Sensor Two in Figure 4.2.

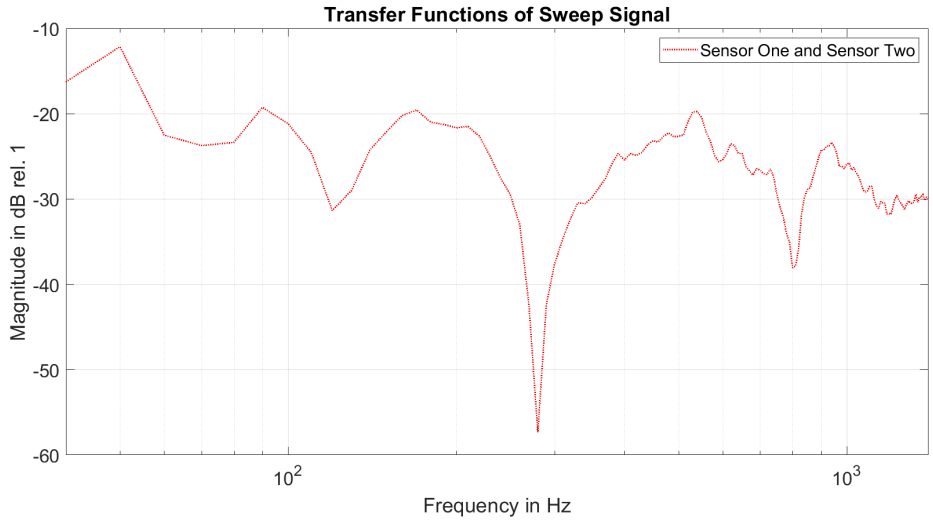

Figure 4.5: Transfer function between the different sensors based on the sweep signal measurement

4.2 Different wrist positions

This section presents the results obtained from the measurements regarding different wrist positions presented in Section 3.3.2. The aim for these measurements was to showcase how the bio-acoustical properties will change depending on how the muscle tension varies depending on the wrist positioning. For this section, the accelerometer located at the radial styloids is referred to as Sensor two while the accelerometer located between sensor two and the force transducer is referred to as Sensor one.

4.2.1 Auto spectrum

The auto spectrum of Sensor one for the different wrist positions, obtained from white noise, can be seen in Figure 4.6. It seems as both extension and flexion caused an increased level in lower frequencies compared to the neutral wrist position, where extension saw the largest increase. All of the wrist positions seems to follow the same shape except for some larger peaks which occurs at 400 Hz and around 1000 Hz for the flexed position.

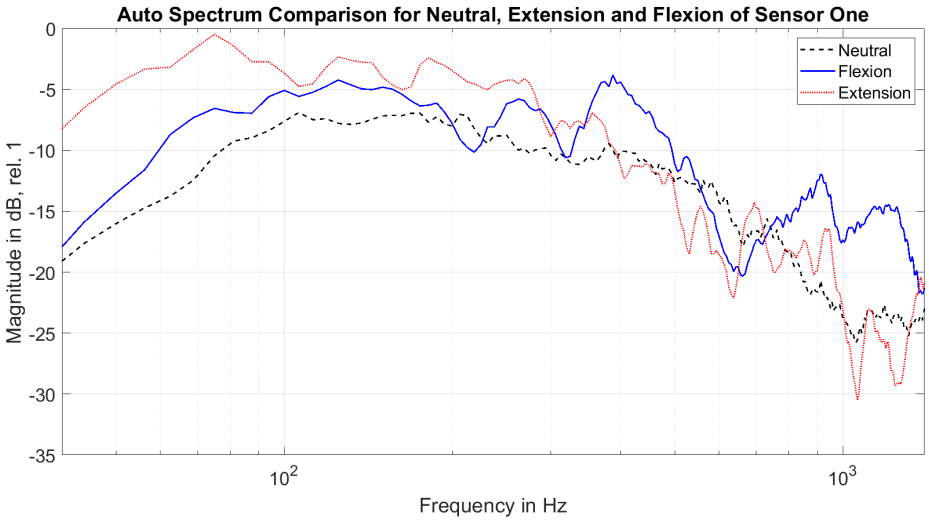

Figure 4.6: Auto spectrum comparison of different wrist positions for Sensor one

Figure 4.7 displays the auto spectrum of Sensor two for the different wrist positions. From this figure it appears as the resonance located at 150 Hz is not present for the other wrist positions. The second resonance around 400 Hz have shifted in frequency for the other wrist positions. For the extension it is now located at 300 Hz, while the flexion has moved towards the region between 600 Hz and 800 Hz.

Figure 4.8 showcases the auto spectrum of Sensor two in third octave bands for the different wrist positions. It is clear that the energy distribution changes depending on the wrist position. The peak seen around 100 Hz disappears for both extension and flexion, while the energy in the lowest frequency bands increase. The overall energy seems to have increased for the extension, except for a dip at 630 Hz which does not exist for the other wrist positions.

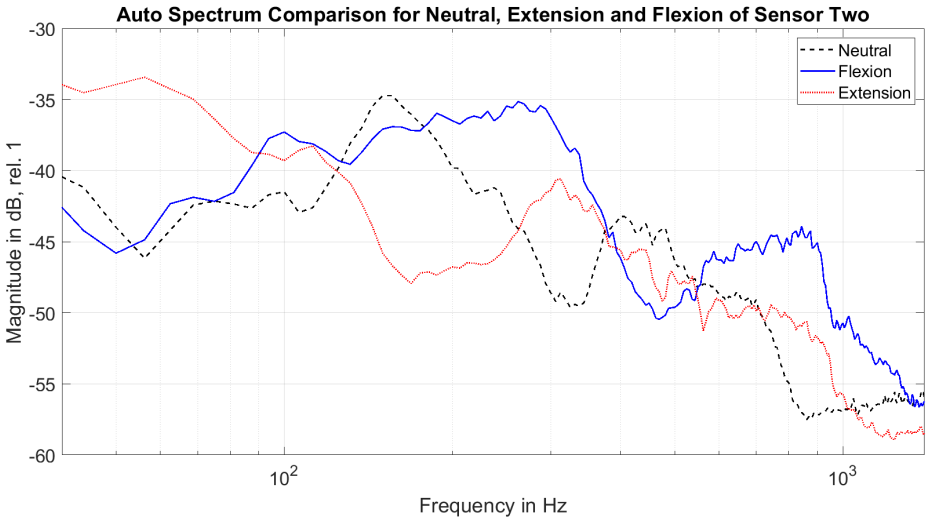

Figure 4.7: Auto spectrum comparison of different wrist positions for Sensor two

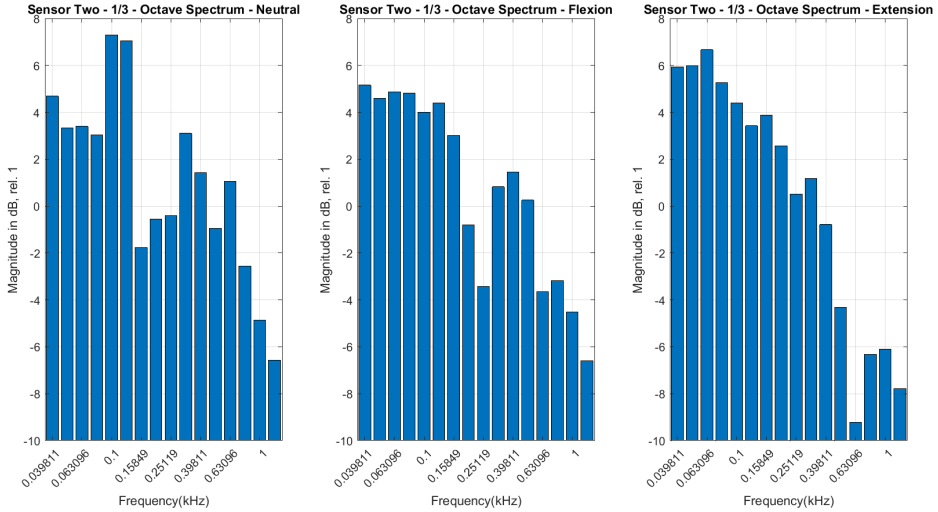

Figure 4.8: Auto spectrum comparison of different wrist positions for Sensor two in 1/3-octave

The auto spectrum for the force transducer, seen in Figure 4.9, reveals that the energy is increased for all frequencies up to 500 Hz for both extension and flexion. Besides this the input energy seems to follow a similar curve.

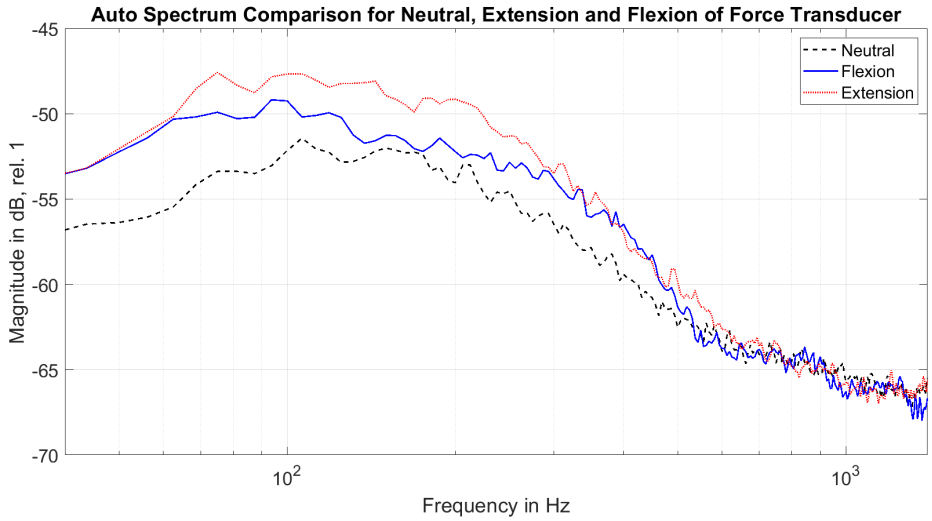

Figure 4.9: Auto spectrum comparison of different wrist positions for Force transducer

4.2.2 Mobility

The input mobility, based on Sensor one, is displayed in Figure 4.10 for all wrist positions. In the lowest frequencies, all of the wrist positions have different levels. For the mid frequencies, flexion varies from the rest with a dip between 370 Hz and 600 Hz. In higher frequencies there are also some level differences, with extension having large peaks above 1000 Hz, not present for the other wrist positions.

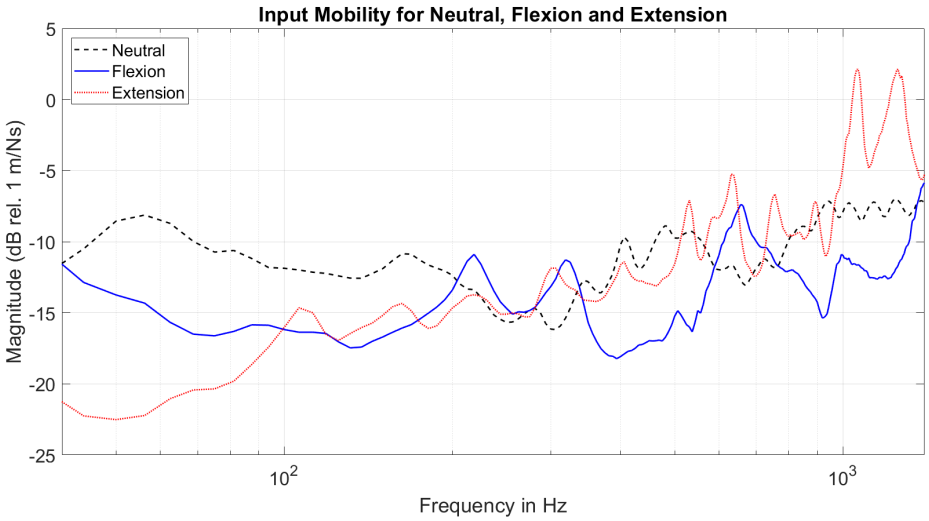

Figure 4.10: Input mobility for the different wrist positions

Figure 4.11 showcases the output mobility for Sensor two. Similar to how the resonances of the auto spectra seen in Figure 4.7, the frequency characteristics appears to shift depending on the wrist position. The peak around 300 Hz seen for the neutral position appears to have shifted towards 180 Hz for the extended wrist position where it also appears to be broader, but for the flexed wrist position this peak seems to have shifted towards 400 Hz. This corresponds to a frequency shift of roughly 30%, which is similar to the 20% expected from Section 2.1.

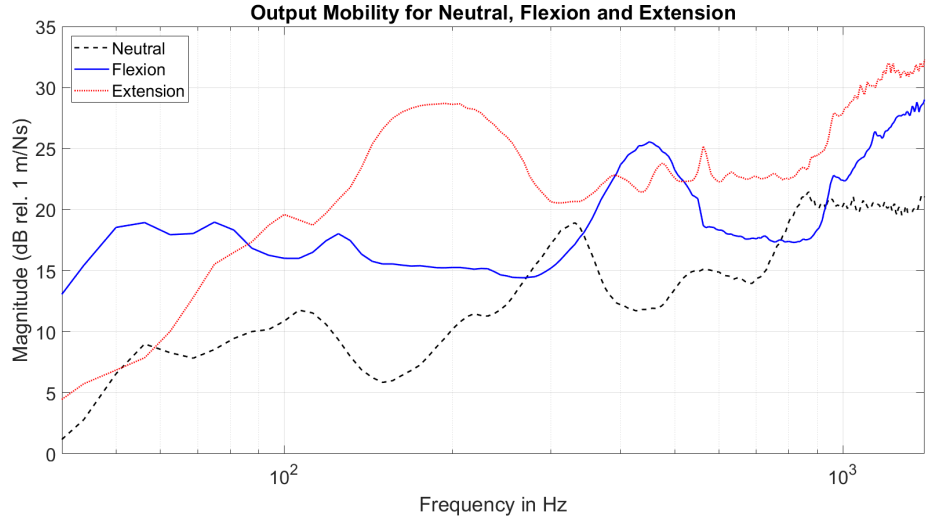

Figure 4.11: Output mobility for the different wrist positions

4.3 Different test subjects

As described in Section 3.3.3, the results in this section consists of measurements conducted on multiple test subjects. This is to see how the bio-acoustical properties of the forearm differs between different individuals. For this section, the accelerometer located at the radial styloids is referred to as Sensor two while the accelerometer located between Sensor two and the force transducer is referred to as Sensor one.

4.3.1 Auto spectra

Figure 4.12 showcases the auto spectrum of Sensor one for all test subjects. The largest difference between the test subjects seems to occur in the lowest frequencies with the exception for Test subject one, which does not share the same slope as the other test subjects in higher frequencies.

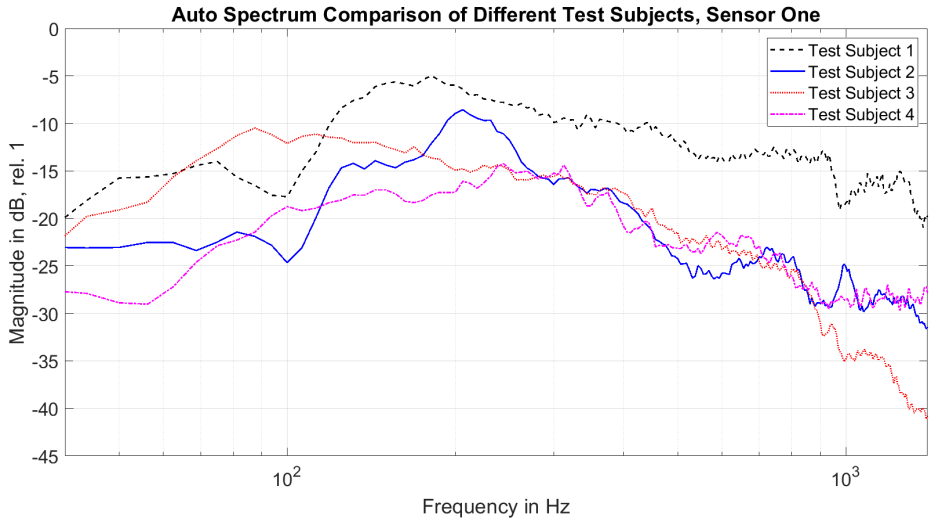

Figure 4.12: Auto spectrum comparison between the different test subjects of Sensor one

The auto spectrum of the Sensor two, seen in Figure 4.13, showcases a frequency region with increased level for all participants. This region differs slightly between the different test subjects in region, width and magnitude, but lies between 70 Hz and 350 Hz. This correlates well with the observed frequency region with the lowest attenuation presented in Section 2.3, which was expected to lie between 150 Hz and 350 Hz.

The variation between the test subjects was unexpected as the test pool is very homogeneous.

Figure 4.13 also showcases a resonance around 600 Hz for Test subject three and a wide region with increased level between 350 Hz and 700 Hz for Test subject four. These are unique for these participants and are not seen for the rest of the test pool, nor do they do match the predicted second resonance at 450 Hz from Section 2.3.

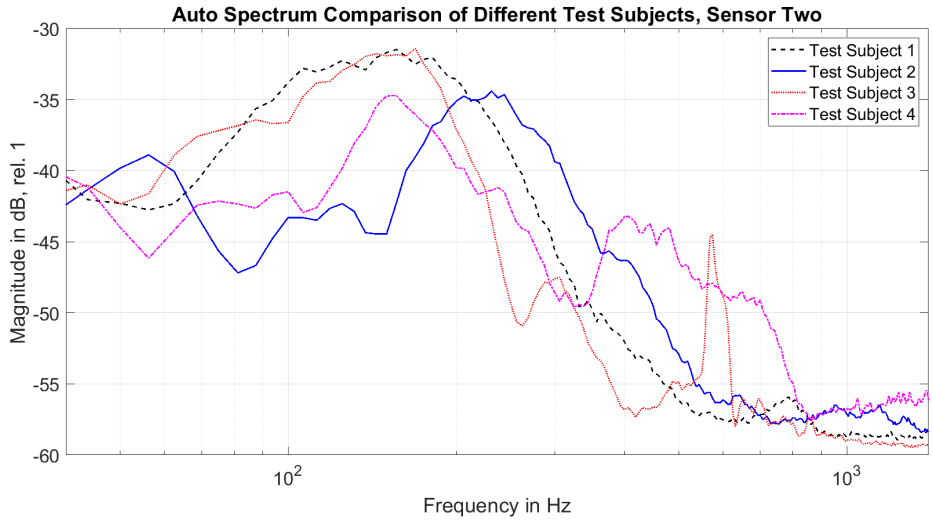

Figure 4.13: Auto spectrum comparison between the different test subjects of Sensor two

4.3.2 Mobility

The input mobility for the different test subjects can be seen in Figure 4.14. Test subject two and Test subject one shares a peak at 100 Hz, which is absent for the other test subjects. All of the test subjects share an increase in mobility for higher frequencies.

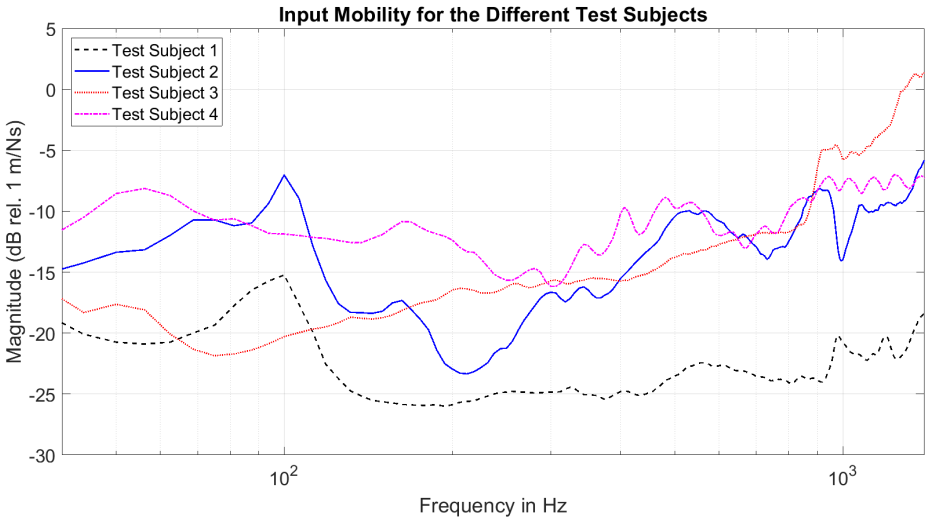

Figure 4.14: Comparison of input mobility for the different test subjects

The transfer mobility displayed in Figure 4.15 showcases that all of the test subjects share a similar shape, where the mobility increases over frequency until it stabilizes between between 500 Hz and 800 Hz. Besides the similarities there are some variations between the subjects as can be seen between 70 Hz and 150 Hz and between 150 Hz and 450 Hz, where changes in mobility only occurs for some of the test subjects. Once again this is unexpected as the test pool is very homogeneous.

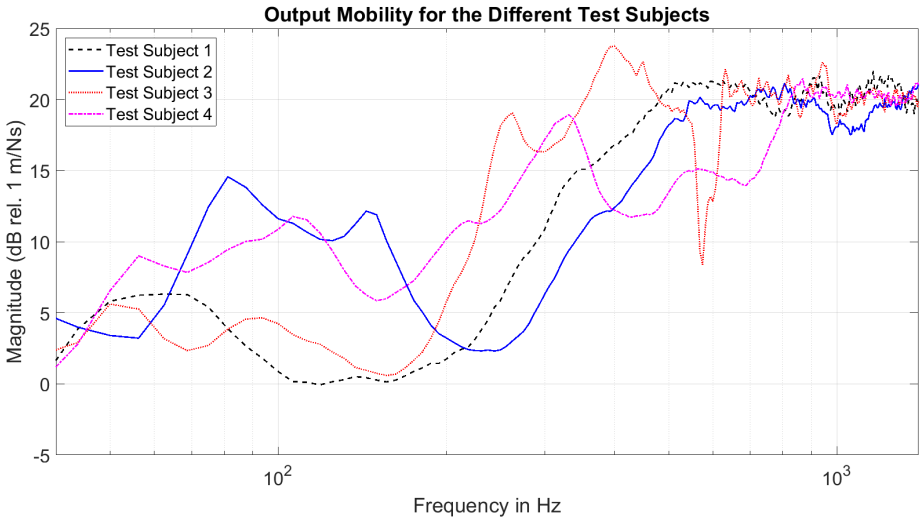

Figure 4.15: Comparison of output mobility for the different test subjects

4.4 Impact measurements

As described in Section 3.3.4, the results presented in this section were obtained through self inflicted impacts on the test subjects forearm. By tapping on the pre-determined impact locations presented in Figure 3.8, the generated bio-acoustical signals were measured by the two sensors located at the wrist in order to analyse the hypothesized location-specific acoustic signatures, discussed in Section 2.1.2.

In this section, the sensor located at the end of the Ulna (specifically at the ulnar styloid) is referred to as Sensor one. The sensor located at the other side of the wrist is referred to as Sensor two, as is depicted in Figure 3.8. The impact locations are also presented in figure 3.8. The impact locations are structured as five rows (going further away from the sensors) and three columns (one at each sensor and one between them).

4.4.1 Comparison between different impact locations

Figure 4.16 showcases the measurement results for both sensors after exciting different impact locations. As expected, the distance from the sensors seems to be the determining factor when it comes to measured amplitude. All of the positions presented in

Figure 4.16 are located at different columns. The sensor located at the same column as the impact detects higher amplitudes compared to the sensor on the opposite side of the wrist, while the impacts occurring on the middle column shows roughly the same amplitude for both sensors. It also seems as the detected impacts becomes lower in energy the further away from the wrist the impact occurred.

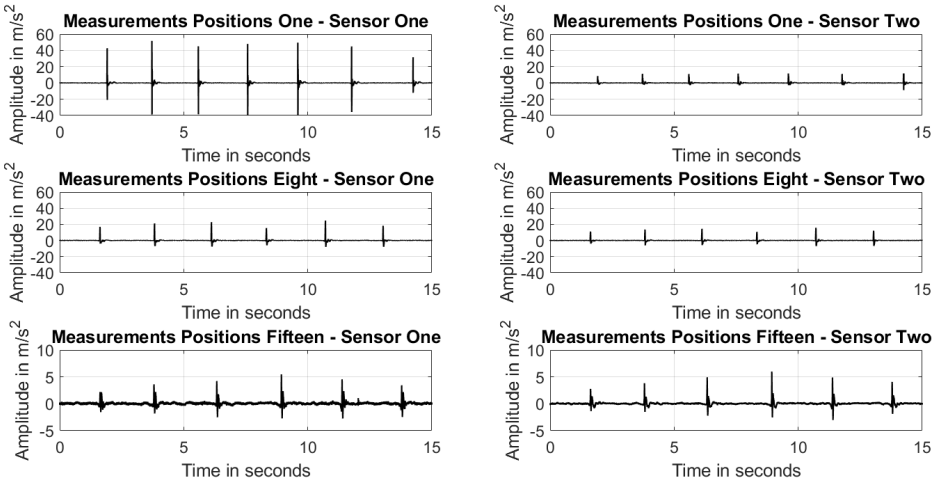

Figure 4.16: Comparison between Sensor one and Sensor two for different impact locations

The spectrogram in Figure 4.17 showcases the same data presented in Figure 4.16. One can see how the majority of the energy from the impacts is present in low frequencies below 100 Hz, and that the higher frequencies are much more prominent when the impacts occur closer to the sensors.

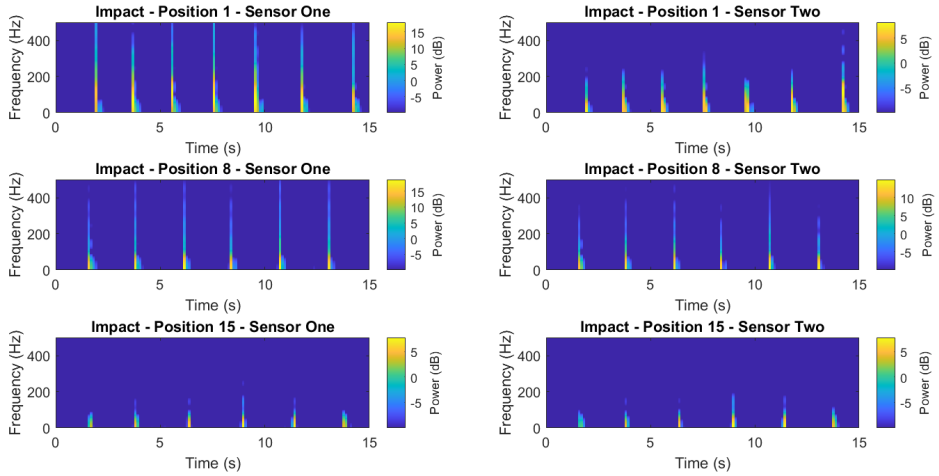

Figure 4.17: Spectrogram comparison between Sensor one and Sensor two for different impact locations

4.4.2 Background noise and signal filtering

Figure 4.18 showcases the background noise of both sensors and it is clear that the level is larger below 100 Hz. As shown in Section 4.4.1, this is also the region where most of the energy from the impacts occur, especially for impacts far from the sensors. Because of this it is unwise to filter out these frequencies. Instead a low pass filter with a cutoff frequency at 450 Hz was applied to the measurement results in order to remove some of the excess energy and thus obtain a cleaner signal.

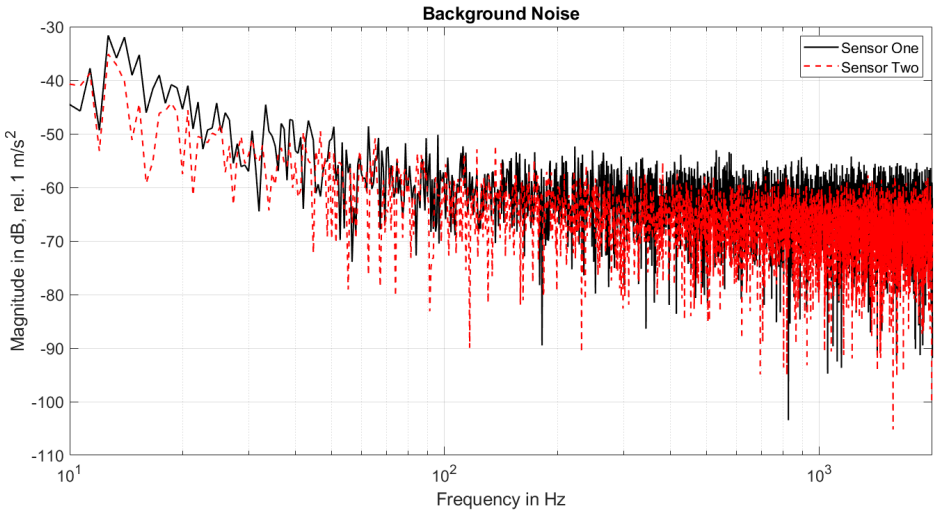

Figure 4.18: Background noise for Sensor one and Sensor two

Figure 4.19 showcases the signal obtained from some impacts at Position fifteen, with and without the low-pass filter. It is clear that the filtering has made the signal less noisy without affecting the amplitude much.

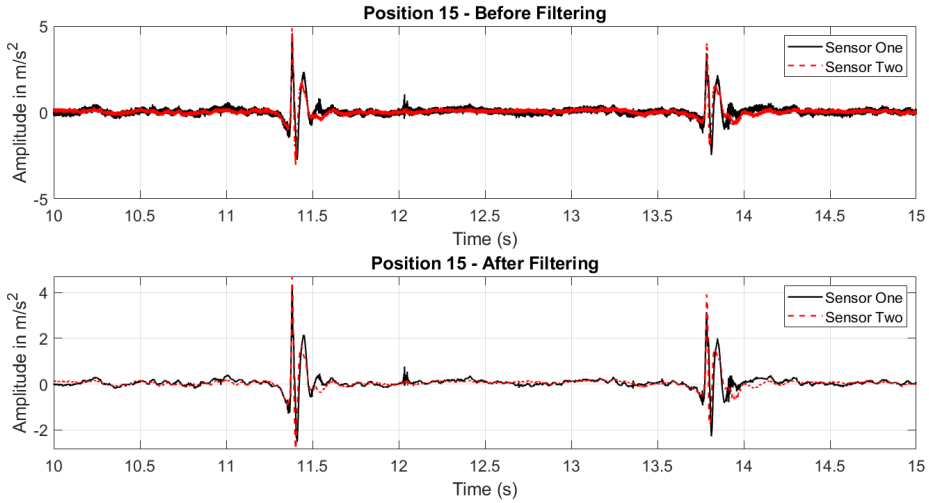

Figure 4.19: Comparison of impact signals at Position fifteen without low-pass filter and with low-pass filter applied

4.4.3 Impact comparison

Figure 4.20 showcases several impacts from Position one as well as an average of these, for both Sensor one and Sensor two. It is clear that besides some small differences in level, the curves are almost identical in shape. As established in Section 4.4.1, the amplitude is larger for Sensor one than for Sensor two because the impact location is closer to Sensor one. Besides the level difference between the two sensors, there is also a distinct difference in their shapes.

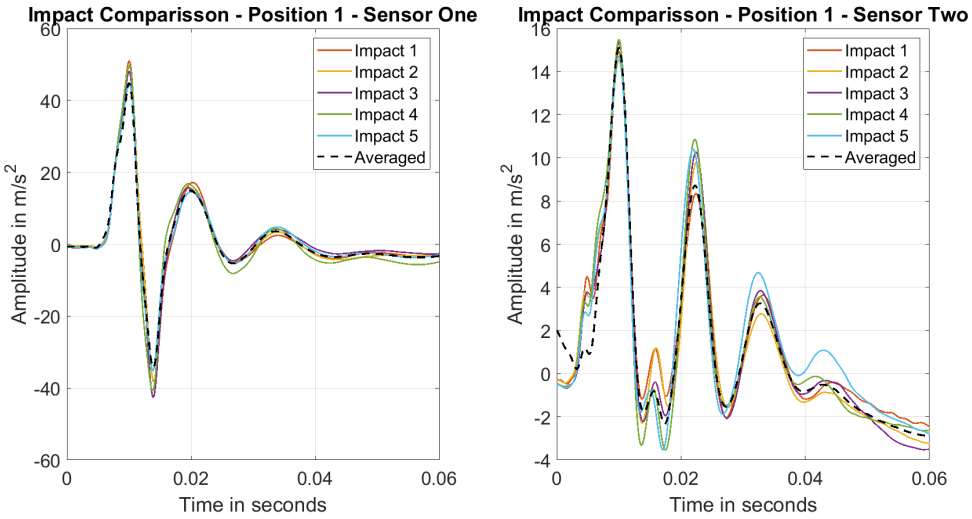

Figure 4.20: Comparison of several impacts of Position one for both Sensors

Similar to Figure 4.20, Figure 4.21 showcases the impacts for Position eight. Once again there is a clear pattern between each impact and a noticeable difference between Sensor one and Sensor two. The level difference between the two sensors is much smaller for this position compared to Position one, which is most likely due to the impact position being located at the same distance from the two sensors.

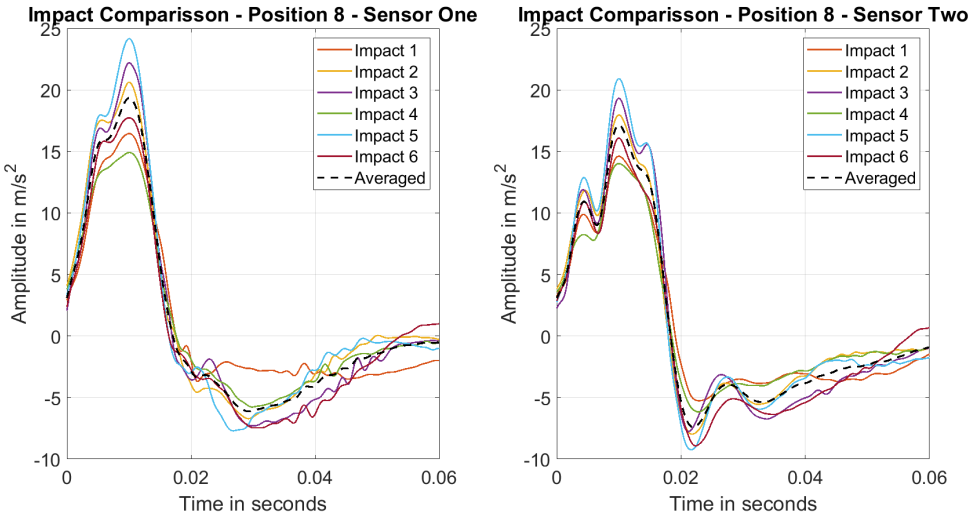

Figure 4.21: Comparison of several impacts for Position eight for both sensors

Figure 4.22 compares several impacts at Position fifteen for both Sensor one and Sensor two. Just as with the other positions, there is a clear difference between the measured impact shape of Sensor one and Sensor two. Even at this distance the level difference is dependent on which side of the forearm the impacts occur. Sensor one seems to be varying more in its shape than what has been seen for previous comparisons. This is probably caused by the distance between the impact location and the sensors, which is much longer compared to previously analyzed positions, and therefore has a weaker signal reaching the sensors.

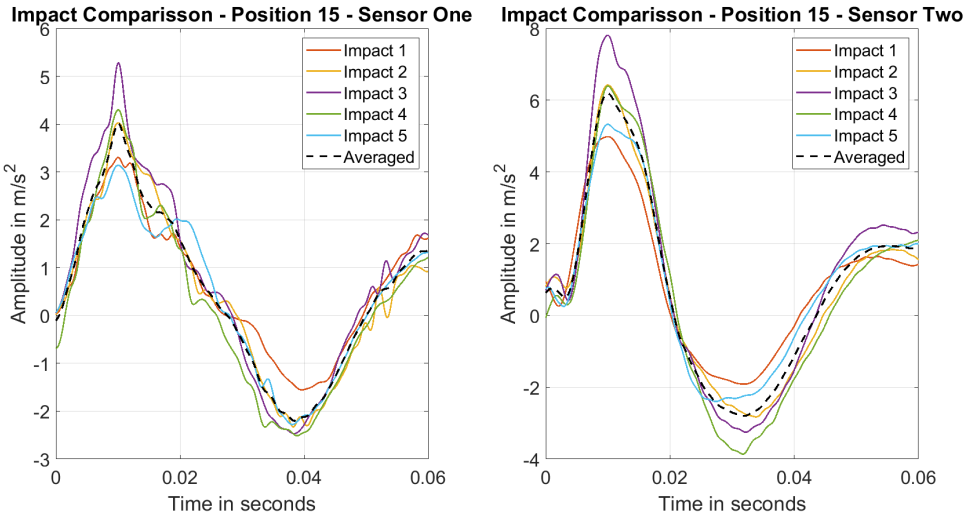

Figure 4.22: Comparison of several impacts for Position fifteen for Sensor one and Sensor two

4.4.4 Comparison of impact locations

Figure 4.23 and Figure 4.24 compares the averaged impact of all positions for Sensor one and Sensor two. The positions are sorted by color which corresponds to the impact rows seen in Figure 3.8.

In Figure 4.23 each impact on Column one is unique. Besides the size and shape of the first peak, there are differences in how large the dip around 0.015 s is compared to the original peak as well as variations in width for all impacts. The rest of the impacts in the other columns also seems to be unique to each other. There does not appear to be any row specific pattern between the columns either. Figure 4.24 also shows unique impacts for all locations over all columns and rows for Sensor two.

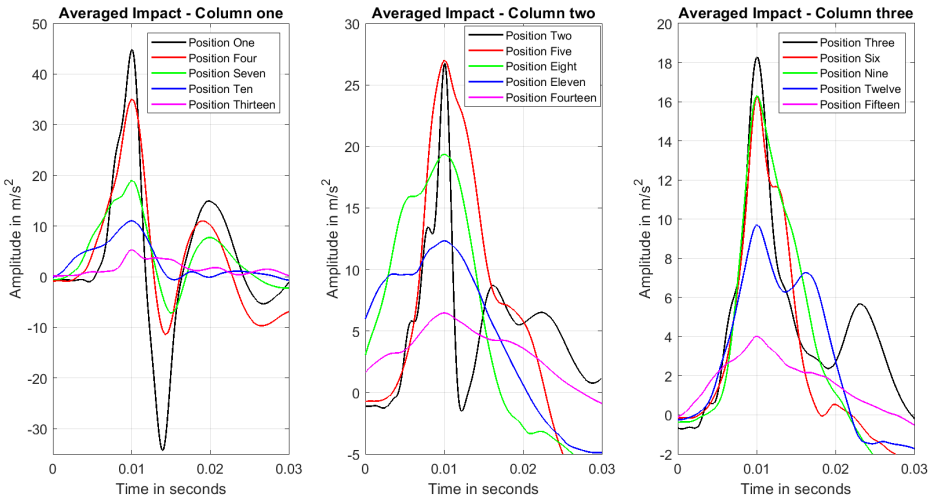

Figure 4.23: Averaged impact of all positions for Sensor one

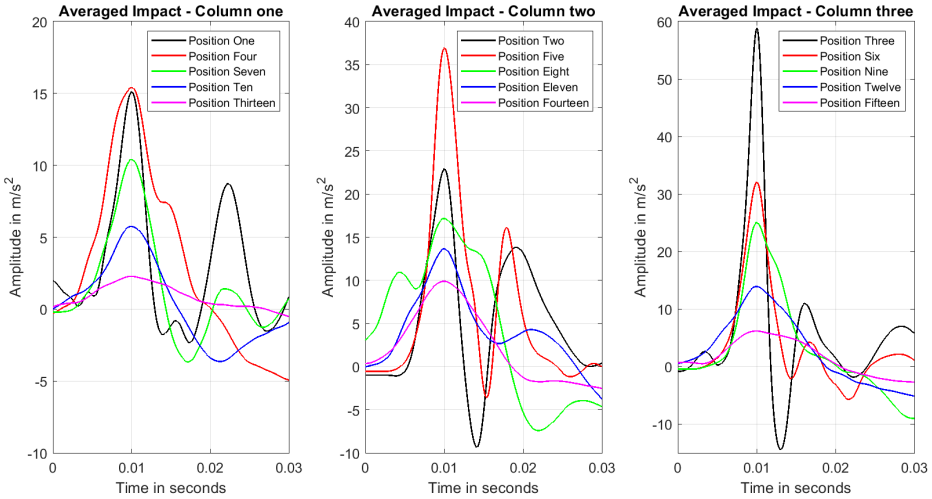

Figure 4.24: Averaged impact of all positions for Sensor two

Table 4.1 showcases the average, minimum and maximum time difference measured between the two sensors for all positions, as well as the standard deviation of the time difference between these impacts.

Column one presents the impact locations at the medial side of the forearm close to the ulna bone. All of the impact of this column reaches Sensor one before Sensor two

with roughly the same time difference, with the exception of Position thirteen. This position also has a much higher range and thus a larger standard deviation compared to the other impacts of this column.

Column three presents the impact locations at the lateral side of the forearm, close to the Radial bone. For the first three impact locations, located closest to Sensor two, all of the impacts reaches Sensor two before Sensor one. Several of the impacts at Position twelve and Position fifteen, located further from the sensors, reaches Sensor one before Sensor two.

For Column two, located at the middle of the forearm, the positions vary in which sensor receives the impact first. Position two, Position five and Position eleven all have the impacts reach Sensor two, Position eight have its impacts reach Sensor one first, and Position fourteen alternates between which sensor the impacts reaches first. Except for Position fourteen, it seems as the positions of Column two are consistent in which sensor the impacts reaches first, as can be seen from their range.

Average Time Difference (Δt = Sensor one - Sensor Two) and Range (min, max) in ms			
Positions	**Impacts Column one**	**Impacts Column two**	**Impacts Column three**
1, 2 and 3	-5,59 [-13.68 -4.14]	1,63 [1,25 2,3]	2,09 [1,29 4,53]
4, 5 and 6	-4,37 [-7,50 -3,09]	1,23 [0,55 2,07]	1,40 [1,02 2,77]
7, 8 and 9	-3,35 [-3,59 -3,09]	-2,40 [-2,73 -1,91]	1,44 [0,70 2,50]
10, 11 and 12	-3,87 [-4,10 -3,59]	4,97 [3,75 6,29]	-1,50 [-3,71 0,35]
13, 14 and 15	-32,83 [-47,89 -14,34]	1,45 [-0,74 6,87]	-0,33 [-2,11 0,90]

Standard Deviation of Time Differences in ms			
Positions	**Impacts Column one**	**Impacts Column two**	**Impacts Column three**
1, 2 and 3	3,57	0,38	1,37
4, 5 and 6	1,57	0,52	0,62
7, 8 and 9	0,19	0,31	0,67
10, 11 and 12	0,24	1,05	1,75
13, 14 and 15	14,95	2,59	1,11

Table 4.1: Time difference between impacts detected by Sensor one and Sensor two

Table 4.2 showcases the amplitude differences between the detected impacts of Sensor one and Sensor two. The table displays a direct comparison, the minimum and

maximum difference, as well as a comparison presented in percentage. Column one and Column three shows that the difference between the the two sensors decreases the further away from the sensors the impact occurs. This is due to the decrease in amplitude over distance as discussed in Section 4.4.1. When comparing the differences in percentage, the amplitude seems to be about twice as large at the sensor located closer to the impact position compared to the sensor furthest away, with the exception of Position one and Position three which are roughly three times as large.

For impacts occurring on Column two, the positions vary in which sensors registers the largest amplitude between impacts, with the exception of Position eight which always provides a larger amplitude for Sensor two. Although Position eight constantly provides a larger amplitude for Sensor two, when comparing the amplitudes of the sensors in percentage it is clear that they are roughly the same. This is true for all Positions except for Position five and Position fourteen, which shows that Sensor one has an averaged amplitude two thirds compared to those of Sensor two.

Average Amplitude difference (Sensor one - Sensor two) and Range (min, max) in ms^{-2}			
Positions	**Impacts Column one**	**Impacts Column two**	**Impacts Column three**
1, 2 and 3	29,86 [15,33 36,00]	3,86 [-9,05 13,46]	-41,29 [-57,07 -29,89]
4, 5 and 6	19,61 [16,99 24,85]	-9,94 [-13,14 -7,01]	-15,79 [-21,50 -8,71]
7, 8 and 9	8,55 [4,91 10,47]	2,20 [0,90 3,25]	-8,73 [-11,92 -3,55]
10, 11 and 12	5,64 [4,237,85]	-1,32 [-4,84 1,88]	-4,50 [-5,33 -3,59]
13, 14 and 15	3,05 [1,03 3,83]	-3,23 [-4,53 -1,36]	-2,18 [-2,53 -1,68]

Comparison of Average Amplitude Difference (Sensor one / Sensor two) in Percentage			
Positions	**Impacts Column one**	**Impacts Column two**	**Impacts Column three**
1, 2 and 3	305	116	31
4, 5 and 6	227	73	50
7, 8 and 9	182	112	65
10, 11 and 12	191	90	69
13, 14 and 15	227	66	64

Table 4.2: Amplitude difference between Sensor one and Sensor two for all impact positions

Figure 4.25 and Figure 4.26 showcases the averaged single sided auto spectrum of several impacts for each position, for both Sensor one and Sensor two. Besides the general pattern consisting of energy decreasing over frequency, each averaged position seems to have unique shapes. As an example, the impacts of Column one for Sensor one seen in Figure 4.25 all have distinct dips occurring between 100 Hz and 450 Hz, with the exception of Position four which does not have any dip before 450 Hz. The actual frequency of where this takes place differs between the impact locations and they also vary in both magnitude and width between each other.

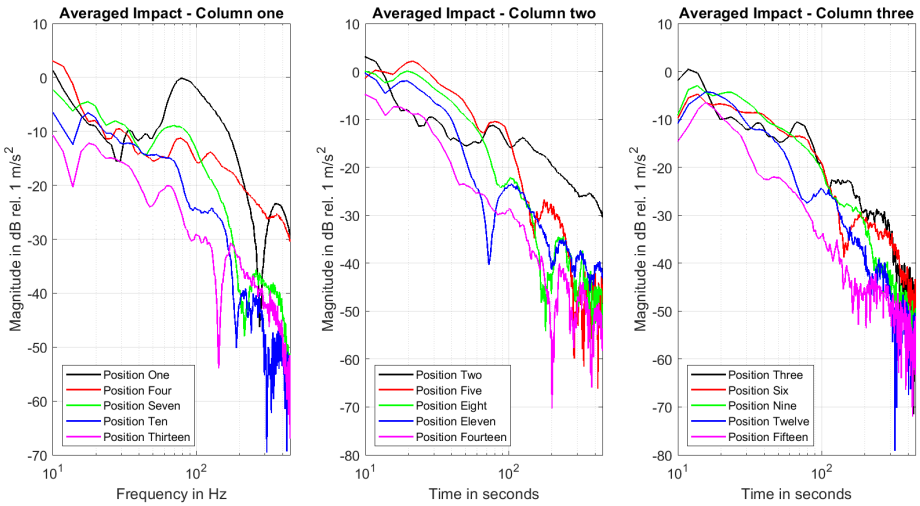

Figure 4.25: Averaged impact of all positions for Sensor one

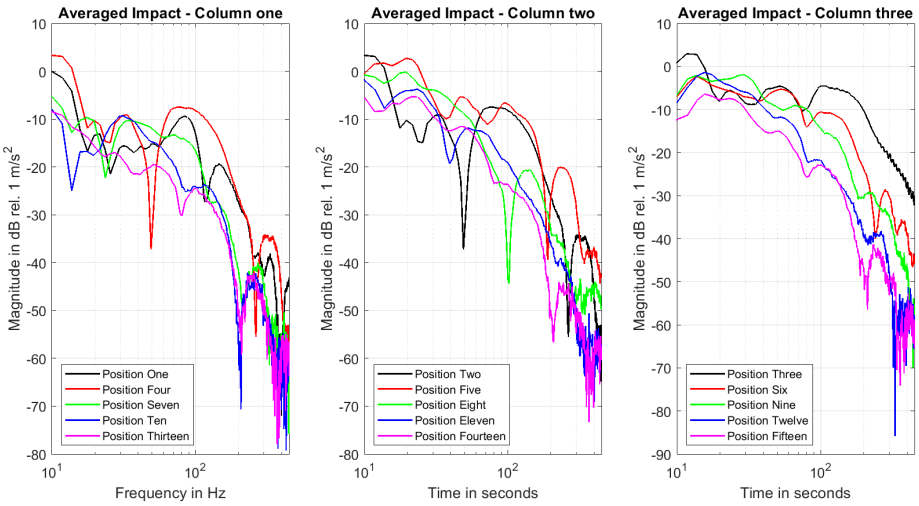

Figure 4.26: Averaged impact of all positions for Sensor one

5 Discussion

5.1 Different test subjects

From the measurements conducted on multiple test subjects seen in Section 4.3, there are clear evidence of a universal characteristics within the test pool, although there are still variations present between the participants. The measurements conducted at the wrist of the test subjects showcased that there is a region with lower attenuation. This frequency region varies somewhat between the test subjects, and can be seen to lie somewhere between 70 Hz and 350 Hz. This corresponds well with the predicted region between 150 Hz and 350 Hz, presented in Section 2.3.

This is also the region where the first resonance of the forearm is expected to occur, both from previous studies related to the bio-acoustics of the forearm seen in Section 2.3, as well as from the calculated resonance obtained through Equation 2.8. Neither the first resonance nor the second resonance predicted to occur around 450 Hz was seen during the measurements. It is possible that the differences in how the measurements were conducted is the reason for the absence of these, as the resonances are based on the long bones and not the whole forearm including the soft tissue, long bones, wrist and coupling between these.

As mentioned there were some discrepancies between the test subjects including resonances at higher frequencies, which did not occur for the rest of the participants. There were also variations between the transfer mobility of the test subjects, although the overall shape with an increased mobility over frequency was a universal characteristics. This was not expected as the test pool was very homogeneous. A larger and more varied test pool is required to obtain better statistical data, as well as to cover a wider range of variations of the bio-acoustical characteristics of the forearm.

5.2 Different wrist positions

The results presented in Section 4.2 showcased how muscle tension caused by wrist movement can affect the frequency characteristics of the forearm. It was found that wrist extension causes the region of least attenuation to be shifted towards lower frequencies, while flexion causes the characteristics to be shifted towards higher frequencies. Both of these wrist positions seems to shift the frequency characteristics with roughly 30%, which is more than the expected 20% presented in Section 2.1. Besides the shift in frequency, the magnitude of the neutral position's resonance seems to be lower compared to both the extended and flexed wrist position. As the results resembles the findings from previous projects presented in Section 2.1, these characteristics are most likely a universal property. As this implies that any subject can adjust the frequency characteristics of its forearm at will, it is possible that this could be utilized by bio-acoustical interfaces to improve or extend the user interface.

5.3 Several impact locations

Just as hypothesised in Section 2.1.1, the different impact locations measured on the forearm seems to have location specific time signatures and frequency spectras. This is most likely what has allowed previous projects to create human-machine interfaces based on bio-acoustics through machine learning algorithms, as was presented in Section 1.1. Although the measured impacts were self inflicted and would thus inherent a large variation in the input force, multiple impacts on the same location were shown to be very similar. It was also found that the majority of the energy from the impacts were located below 450 Hz for all impact locations.

A symmetrical pattern was found when comparing the measured amplitude between the two sensors located at the wrist for the same impact. The ratio between the amplitudes of the two sensors were mirrored over the lateral and medial side of the forearm, which gave these locations unique amplitude ratios. Impacts occurring at the center of the forearm does not show a consistent pattern. These impacts also shared the same amplitude ratio as some of the impacts on the lateral and medial side. This means that location specific ratio does not exist if the potential impact locations also includes the middle of the forearm.

The symmetrical pattern of the amplitude ratios was not seen for the averaged time difference between the sensors. This indicates that the bio-acoustical vibrations find complex paths between the impact locations and the sensors, causing the distance to not be the only parameter dictating how long it takes for vibrations to reach the sensor. There were also several impact locations with the same time difference, making it impossible to determine the direction of arrival from the time difference itself.

6 Conclusion and further research

As shown in this project, different positions of the forearm seems to have unique bio-acoustical properties in both time domain and frequency domain, which can be utilized to determine the source of the impact. The amplitude difference between two sensors at the forearm seems to by itself be able to determine the source of arrival for locations located at the lateral and medial side of the forearm. However, it will only work if impact locations at the middle of the forearm are excluded. Time difference between the two sensors is not reliable enough to determine the direction of arrival by itself.

The bio-acoustical characteristics seems to be somewhat universal between different test subjects, although more measurements need to be conducted on a larger and less homogeneous test pool in order to obtain statistical data. There is a sweet spot for bio-acoustical measurements of the forearm between 70 Hz and 150 Hz, although the bio-acoustical properties of a individual's forearm was found to be altered by flexing or extending the wrist.

The findings of this study is a good start for mapping and understanding the bio-acoustics of the forearm. However, the measurements conducted during this thesis are few and not sufficient to provide statistical data. Further research is needed on a larger and less homogeneous test pool in order to truly understand the universal bio-acoustical characteristics of the forearm. A larger data set of forearm impacts would also be of interest, as this could be used to construct an algorithm which determines the impact location based on the multitude of parameters discussed in this thesis.

References

[1] T. Deyle, S. Palinko, E. S. Poole, and T. Starner, "Hambone : A Bio-Acoustic Gesture Interface," 2007.

[2] L. Zhong, D. El-Daye, B. Kaufman, N. Tobaoda, T. Mohamed, and M. Liebschner, "OsteoConduct: Wireless body-area communication based on bone conduction," *BODYNETS 2007 - 2nd International ICST Conference on Body Area Networks*, pp. 1–8, 2007.

[3] C. Harrison, D. Tan, and D. Morris, "Skinput: Appropriating the skin as an interactive canvas," *Communications of the ACM*, vol. 54, no. 8, pp. 111–118, 2011.

[4] O. Jones, "The Wrist Joint - TeachMeAnatomy," 2021.

[5] BoneFixator, "Anatomy of the long bone," 2007.

[6] J. M. Jurist, "In vivo determination of the elastic response of bone. II. Ulnar resonant frequency in osteoporotic, diabetic and normal subjects," *Physics in Medicine and Biology*, vol. 15, no. 3, pp. 427–434, 1970.

[7] Clayton Rich, Eli Klink, Ray Smith, Ben Graham, and Peter Ivanovich, "Progress in Development of Methods in Bone Densitometry - Google Böcker," in *Washington, Scientific and Technical Information Division, National Aeronautics and Space Administration* (G. Donals Whedon, William F. Neuman, and Dale W. Jenkins, eds.), (Washington D.C), pp. 137–144, Scientific and Technical Information Division, National Aeronautics and Space Administration, 5 1966.

[8] Chalmers Univerity of Technology, "Lab 5: Basic Vibration Measurements Sound and Vibration Measurements," 11 2019.

[9] P. H. Nicholson, P. Moilanen, T. Kärkkäinen, J. Timonen, and S. Cheng, "Guided ultrasonic waves in long bones: Modelling, experiment and in vivo application,"

Physiological Measurement, vol. 23, pp. 755–768, 11 2002.

[10] A. Tatarinov, N. Sarvazyan, and A. Sarvazyan, "Use of multiple acoustic wave modes for assessment of long bones: Model study," 2005.

[11] T. Irvine, "FORMULAS FOR CALCULATING THE SPEED OF SOUND Revision G," tech. rep., 2000.

[12] Lawrence F. Kinsler, Austin R. Frey, Alan B. Coppens, and James V. Sanders, *Fundamentals of Acoustics*. 4 ed., 2000.

[13] H. Aygün, C. Barlow, L. Yule, and S. Y. Liu, "Sound propagation through bone tissue," *Proceedings of the Institute of Acoustics*, vol. 37, pp. 234–238, 2015.

[14] M. Cerna and A. F. Harvey, "National Instruments Application Note 041," tech. rep., 2000.

[15] J. Ahrens, P. Andersson, T. Johansson, S. Kleiven, and W. Kropp, "Sound and Vibration Measurements (SVM) Lab 4: The H1-Estimator," tech. rep., 2020.

[16] O. Døssing and B. . Kjae, "STRUCTURAL TESTING Part I: Mechanical Mobility Measurements," tech. rep., Brüel & Kjaer, 1998.

[17] "Mobility Measurements," tech. rep.

Department of Civil and Environmental Engineering
CHALMERS UNIVERSITY OF TECHNOLOGY
Gothenburg, Sweden
www.chalmers.se

CHALMERS